

YANJUN XIN<sup>1,2</sup>, GANG WANG<sup>2</sup>, YONGPING LIU<sup>3</sup>, ZHILIN ZANG<sup>2</sup>, MENGCHUN GAO<sup>1</sup>

## EFFECT OF WO<sub>3</sub> ON THE MORPHOLOGY AND PHOTODEGRADATION OF DIMETHYL PHTHALATE OF TiO<sub>2</sub> NANOTUBE ARRAY PHOTOELECTRODE

WO<sub>3</sub> modified TiO<sub>2</sub> nanotube array (WO<sub>3</sub>/TNAs) photoelectrodes were fabricated via electrochemical deposition on TNAs/Ti photoelectrodes. The morphology and structure of WO<sub>3</sub>/TNAs photoelectrodes were investigated by scanning electron microscopy (SEM) and X-ray diffractometer (XRD). The effects of deposition potential, deposition duration, Na<sub>2</sub>WO<sub>4</sub> concentration, and calcination temperature on the morphology and the photocatalytic activity were investigated. The results showed that suitable amounts of WO<sub>3</sub> promoted the photocatalytic activity of TNAs photoelectrodes for the degradation of dimethyl phthalate (DMP). The optimal conditions for the fabrication of WO<sub>3</sub>/TNAs photoelectrodes were as follows: deposition voltage 3.0 V, 10 min deposition duration, 0.01 mol/dm<sup>3</sup> Na<sub>2</sub>WO<sub>4</sub> concentration, 1.5 cm electrode gap, and 550 °C annealing temperature. The degradation rate of DMP reached 77% after 60 min of illumination by WO<sub>3</sub>/TNAs photoelectrode. Additionally, WO<sub>3</sub>/TNA photoelectrodes possessed superb stability for maintaining a high DMP degradation efficiency at more than 75% after 10 times of successive use with 60 min irradiation for each cycle. The enhancement of photocatalytic performance by the efficient combination of WO<sub>3</sub> with TNAs would provide a theoretical basis for the practical application of WO<sub>3</sub>/TNA photoelectrodes in water treatment.

### 1. INTRODUCTION

Phthalates (PAEs) are widely used as a plasticizers in industry. As one kind of PAEs, dimethyl phthalate (DMP) could accumulate in biological organisms and disturb the endocrine system even at a low concentration. DMP is a ubiquitous environmental pollutant and is listed as one of the priority pollutants by American EPA as well as by

---

<sup>1</sup>The Key Laboratory of Marine Environmental Science and Ecology, Ministry of Education, Ocean University of China, Qingdao, 266003, China, corresponding author Y. Xin, e-mail address: xintom2000@126.com

<sup>2</sup>Qingdao Engineering Research Center for Rural Environment, College of Resource and Environment, Qingdao Agricultural University, Qingdao 266109, China.

<sup>3</sup>College of Science and Information, Qingdao Agricultural University, Qingdao 266109, China.

China's Ministry of Environmental Protection. Therefore, investigating methods for DMP degradation is critically important. Several such methods including photocatalytic oxidation [1–3], electrochemical degradation [4, 5], adsorption [6, 7] and sonoelectrolysis [8, 9] have been investigated.

In the last decade, TiO<sub>2</sub> nanotube arrays (TNAs) have received intense attention. They are considered one of the most promising photocatalysts for their remarkable ability of charge transport and superior oxidation [10–12]. However, TNAs photocatalysts, with band gap of 3.0–3.2 eV, could be activated only by UV radiation ( $\lambda < 380$  nm) which accounts to less than 5% of solar energy on the Earth's surface [13].

To use the sunlight in an efficient way for TNAs photocatalyst, various doping materials have been used, such as C [14, 15], Pd [16], In [17], Bi [18], CdTe [19], CdS [20, 21], WO<sub>3</sub> [22] and Sb<sub>2</sub>S<sub>3</sub> [23]. It is well known that WO<sub>3</sub> has a slightly lower conduction band (CB) than that of TiO<sub>2</sub>, thus the photoelectrons could transfer from the CB of TiO<sub>2</sub> to the CB of WO<sub>3</sub> and the recombination of charge carriers is reduced [22].

In our previous study [24, 25], WO<sub>3</sub> was successfully incorporated onto TNAs surface by a convenient cycle pulse electrodeposition method in tungstate solution. In this research, the effects of deposition potential, the Na<sub>2</sub>WO<sub>4</sub> concentration and the annealed temperature on the photodegradation of DMP were investigated.

## 2. EXPERIMENTAL

*Chemicals and materials.* Titanium foils (purity > 99.9%, 0.2 mm thick) were obtained from Baoji Titanium and Nickel Manufacture Limited Company, China. All chemicals were obtained as analytical reagent grade and used without further purification. The experimental solutions were prepared with doubly distilled water.

*Sample preparation and characterization.* The TNAs photoelectrode (20×10 mm) fabricated by our group [12] and platinum (Pt) sheet were separately used as a cathode and anode in 0.1 mol/dm<sup>3</sup> Na<sub>2</sub>SO<sub>4</sub> solution with various amounts of Na<sub>2</sub>WO<sub>4</sub> (0.002, 0.005, 0.01, 0.03, 0.05 mol/dm<sup>3</sup>). The deposition process was conducted at various potentials (1, 3 and 5 V) and times (2–60 min). Then the samples were immediately rinsed with deionized water and dried at 378 K for 60 min. Finally the photoelectrodes were annealed at 400 °C, 550 °C, 600 °C and 700 °C each for 120 min. The surface morphology of fabricated photoelectrodes was studied by SEM (America QUANTA200F). The crystal structure was examined using X-ray diffractometer (XRD, Rigaku D/max-rb) with CuK<sub>α</sub> radiation ( $\lambda = 1.5418$ ) at 0.02° intervals of  $2\theta$  over the range of 10–90°.

*Photocatalytic activity.* The photocatalytic performance of WO<sub>3</sub>/TNAs photoelectrode was investigated using DMP aqueous solution (40 cm<sup>3</sup>) in a single-compartment cylindrical quartz reactor. The concentration of DMP was 20 mg/dm<sup>3</sup>. Before photoreaction,

the sample solution was stirred in the dark for 30 min to reach adsorption/desorption equilibrium, then the sample solution, under magnetic stirring, was illuminated. A 75 W xenon lamp of was used as an external light source with the light intensity of 30.5 mW/cm<sup>2</sup> which would last 60 min. The DMP solution was collected at specific time intervals and analyzed immediately. The concentration of DMP was determined by the high performance liquid chromatography (HPLC, LC-20A, Shimadzu, Japan) with Inertsil ODS-SP column (150×4.6 mm, 5 μm). The detection optical wavelength was 228 nm. The mobile phase was mixture of methanol with water (9:1) with the flow rate of 1.0 cm<sup>3</sup>/min. The column temperature was 30 °C.

The degradation rate of DMP was calculated using the following formula:

$$D = \frac{C_0 - C}{C_0} \times 100\% \quad (1)$$

where  $C_0$  is the initial concentration,  $C$  is the concentration after a certain period of illumination.

### 3. RESULTS AND DISCUSSIONS

#### 3.1. MORPHOLOGY AND CRYSTAL STRUCTURE

Figure 1 shows the morphology of WO<sub>3</sub>/TNAs photoelectrodes fabricated at various deposition potentials in 0.01 mol/dm<sup>3</sup> Na<sub>2</sub>WO<sub>4</sub> and 0.1 mol/dm<sup>3</sup> Na<sub>2</sub>SO<sub>4</sub>.

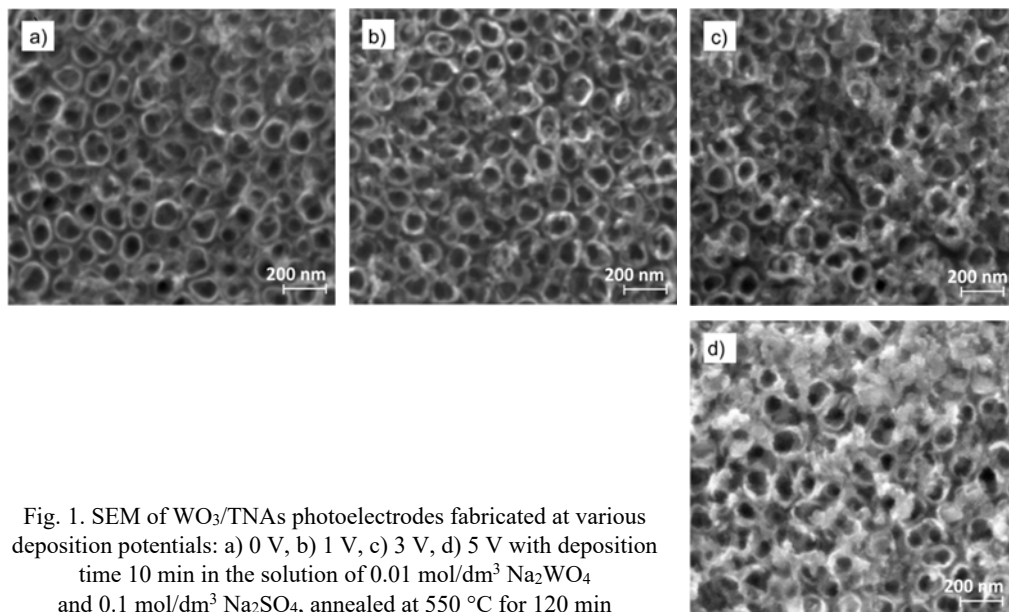


Fig. 1. SEM of WO<sub>3</sub>/TNAs photoelectrodes fabricated at various deposition potentials: a) 0 V, b) 1 V, c) 3 V, d) 5 V with deposition time 10 min in the solution of 0.01 mol/dm<sup>3</sup> Na<sub>2</sub>WO<sub>4</sub> and 0.1 mol/dm<sup>3</sup> Na<sub>2</sub>SO<sub>4</sub>, annealed at 550 °C for 120 min

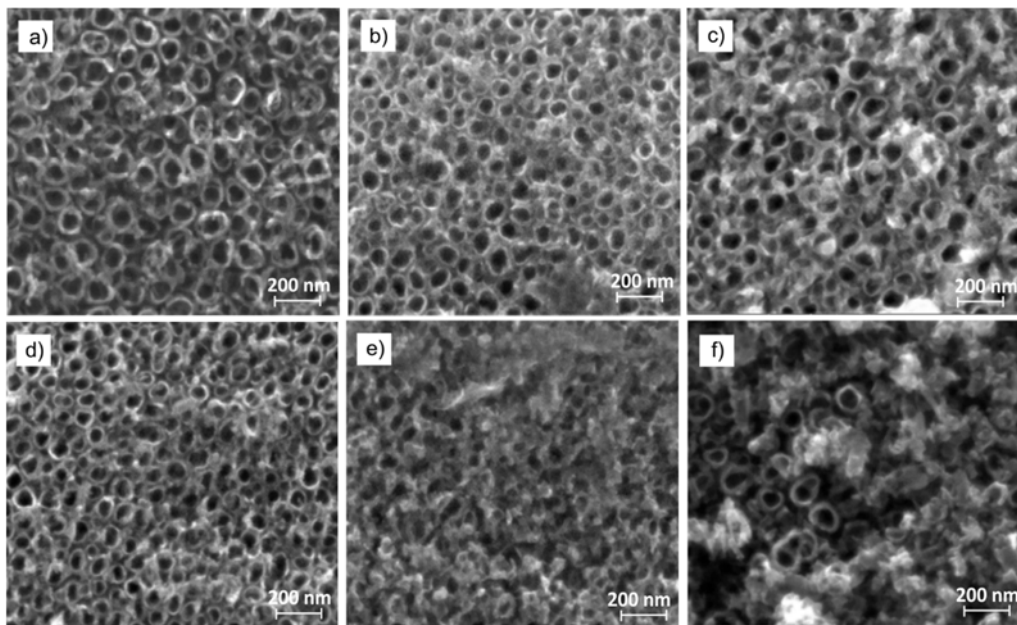


Fig. 2. SEM of  $\text{WO}_3/\text{TNAs}$  photoelectrodes fabricated at various  $\text{Na}_2\text{WO}_4$  concentrations: a) 0, b) 0.002 mol/dm<sup>3</sup>, c) 0.005 mol/dm<sup>3</sup>, d) 0.01 mol/dm<sup>3</sup>, e) 0.03 mol/dm<sup>3</sup>, f) 0.05 mol/dm<sup>3</sup> with the deposition time 10 min, deposition potential 3 V, annealed at 550 °C for 120 min

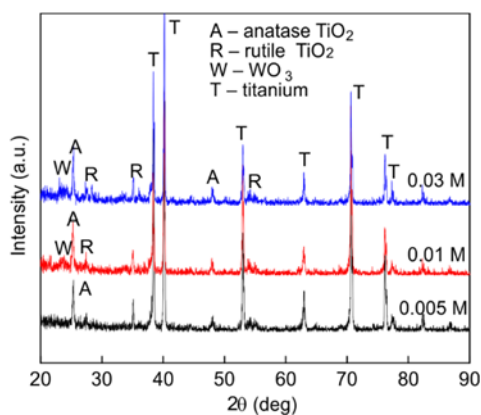


Fig. 3. XRD of  $\text{WO}_3/\text{TNAs}$  photoelectrodes fabricated at various  $\text{Na}_2\text{WO}_4$  concentrations with the deposition time 10 min, deposition potential 3 V, annealed at 550 °C for 120 min

The results showed that all  $\text{WO}_3/\text{TNAs}$  photoelectrodes have ordered nanotube arrays with the tube diameter of 90–100 nm and the wall thickness of 13–15 nm. There was no obvious difference between the photoelectrodes fabricated at 0 V and 1 V (Figs. 1a and 1b). However, the sediment was clearly present on the top of nanotube arrays when the deposition potential was 3 V (Fig. 1c). When the deposition potential was 5 V (Fig. 1d), some tubes were blocked. The results in Fig. 1 indicate that as the

deposition potentials increased, the sediment gradually increased as well. The morphology of WO<sub>3</sub>/TNAs photoelectrode fabricated at various Na<sub>2</sub>WO<sub>4</sub> concentrations is shown in Fig. 2. The crystal structure of WO<sub>3</sub>/TNAs photoelectrode annealed at 550 °C for 120 min is shown in Fig. 3.

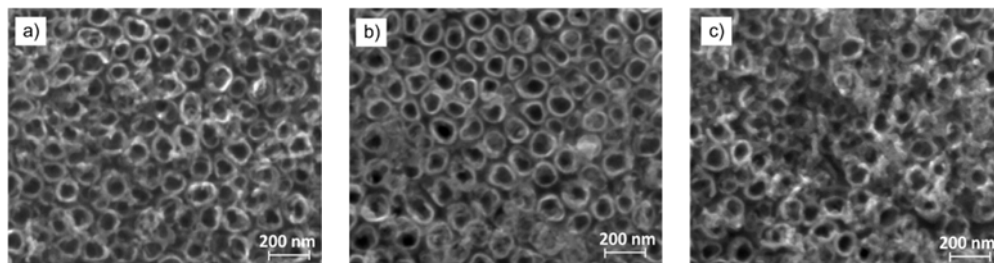


Fig. 4. SEM of WO<sub>3</sub>/TNAs photoelectrodes fabricated at various deposition times: a) 0 min, b) 5 min, c) 10 min, d) 20 min, e) 60 min with the deposition potential 3 V, Na<sub>2</sub>WO<sub>4</sub> concentration of 0.01 mol/dm<sup>3</sup>, annealed at 550 °C for 120 min

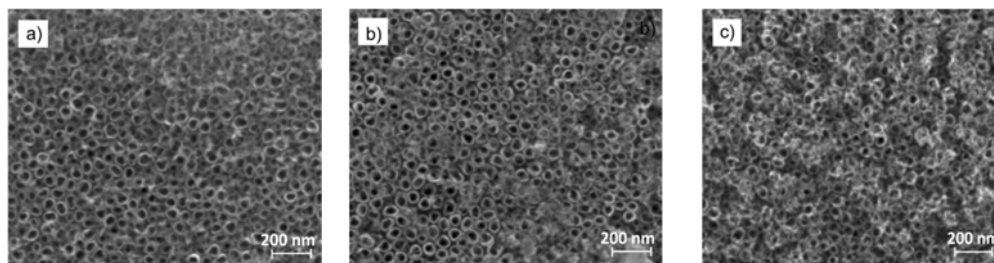


Fig. 5. SEM of WO<sub>3</sub>/TNAs photoelectrodes fabricated at various annealing temperatures: a) unannealed, b) 400 °C, c) 550 °C, d) 600 °C, e) 700 °C with the deposition potential 3 V, deposition time 10 min, and Na<sub>2</sub>WO<sub>4</sub> concentration 0.01 mol/dm<sup>3</sup>

The results show that with an increasing concentration of Na<sub>2</sub>WO<sub>4</sub>, the sediment on the top of nanotube array gradually increased (Figs. 2a–d). When the concentration

of  $\text{Na}_2\text{WO}_4$  was  $0.03 \text{ mol/dm}^3$ , some nanotubes were blocked (Fig. 2e). A thick sediment covered the surface of nanotube array when the concentration of  $\text{Na}_2\text{WO}_4$  increased to  $0.05 \text{ mol/dm}^3$  (Fig. 2f). In Figure 3, a characteristic peak of  $\text{WO}_3$  was found at  $23.5^\circ$  when the concentration of  $\text{Na}_2\text{WO}_4$  increased from  $0.01$  to  $0.03 \text{ mol/dm}^3$  which indicated that  $\text{WO}_3$  was incorporated successfully onto TNAs. When the concentration of  $\text{Na}_2\text{WO}_4$  was low at  $0.002 \text{ mol/dm}^3$ ,  $\text{WO}_3$  was not detected. As the  $\text{Na}_2\text{WO}_4$  concentration increased, the amounts of  $\text{WO}_3$  incorporated onto TNAs increased as well.

The morphology of  $\text{WO}_3/\text{TNAs}$  photoelectrodes annealed at various temperatures is shown in Fig. 5. The morphology of  $\text{WO}_3/\text{TNAs}$  photoelectrode annealed at  $400^\circ\text{C}$  showed no difference with that of unannealed photoelectrodes (Figs. 5a–b, respectively). When the photoelectrode was annealed at  $550^\circ\text{C}$  or  $600^\circ\text{C}$ , some fine particles emerged on the surface (Figs. 5c–d) for the aggregation of  $\text{WO}_3$ . When the annealed temperature was  $700^\circ\text{C}$ , the nanotube collapsed and turned to worm state (Fig. 5e).

### 3.2. PHOTOCATALYTIC PERFORMANCE

The photodegradation rates of  $\text{WO}_3/\text{TNAs}$  photoelectrodes fabricated at various deposition potentials are shown in Fig. 6. When the deposition potential was lower than  $3.0 \text{ V}$ , upon its increase the photodegradation rate of DMP increased too and reached the peak of  $82.6\%$ . The degradation rate of DMP decreased when the potential exceeded  $3.0 \text{ V}$ .

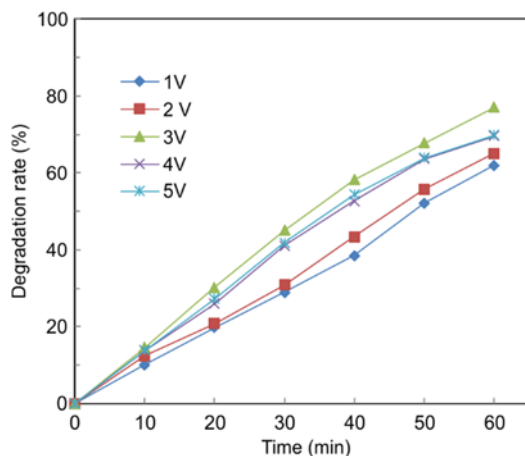


Fig. 6. Time dependences of the evolution of DMP photodegradation rate for  $\text{WO}_3/\text{TNAs}$  photoelectrodes fabricated at various deposition potentials; deposition time  $10 \text{ min}$ ,  $\text{Na}_2\text{WO}_4$  concentration  $0.01 \text{ mol/dm}^3$ , initial DMP concentration  $20 \text{ mg/dm}^3$ , and annealing temperature  $550^\circ\text{C}$

The amount of  $\text{WO}_3$  sediment on the surface of TNAs increased gradually with the increase of the deposition potential (Fig. 1). Compared with TNAs,  $\text{WO}_3$  could absorb much more light and would trap the photogenerated electrons. Thus, the light quantum

efficiency was enhanced. However, too much WO<sub>3</sub> would block the mouth of nanotubes (Fig. 1) and therefore inhibited the light adsorption and the transfer of photogenerated electrons of TNAs, leading to a decreased rate of DMP photodegradation. The results verified that suitable amounts of WO<sub>3</sub> were beneficial to the photocatalytic activity of TNAs photoelectrode.

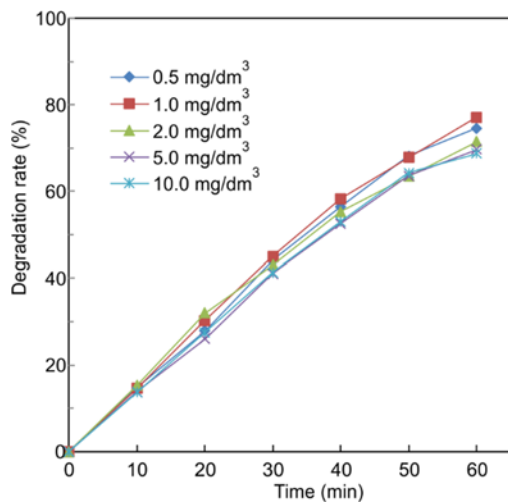


Fig. 7. Time dependences of the DMP photodegradation rate for WO<sub>3</sub>/TNAs photoelectrodes fabricated at various concentrations of Na<sub>2</sub>WO<sub>4</sub>, deposition time 10 min, deposition potential 3 V, annealing temperature of 550 °C, initial DMP concentration 20 mg/dm<sup>3</sup>

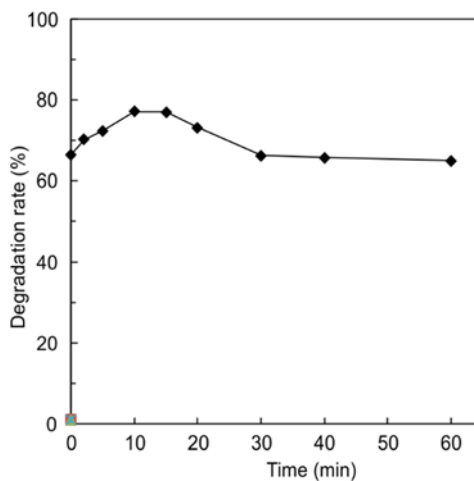


Fig. 8. Time dependences of the DMP photodegradation rate for WO<sub>3</sub>/TNAs photoelectrodes fabricated at Na<sub>2</sub>WO<sub>4</sub> concentration of 0.01 mol/dm<sup>3</sup>, deposition potential 3 V, annealing temperature 550 °C, initial DMP concentration 20 mg/dm<sup>3</sup>

Figure 7 presents the photodegradation rates of DMP for WO<sub>3</sub>/TNAs photoelectrodes fabricated at various Na<sub>2</sub>WO<sub>4</sub> concentrations. The degradation rate of DMP increased when the concentration of Na<sub>2</sub>WO<sub>4</sub> increased at the range of 0–0.01 mol/dm<sup>3</sup>. The photodegradation rate decreased when the concentration of Na<sub>2</sub>WO<sub>4</sub> exceeded 0.01 mol/dm<sup>3</sup>. This agreed with previous experiments (Fig. 6) which showed that redundant WO<sub>3</sub> became the recombination centers of photogenerated electron-hole pairs and inhibited the light absorption of TNAs. Therefore, superfluous WO<sub>3</sub> would undermine the photodegradation rate of DMP for WO<sub>3</sub>/TNAs photoelectrode.

Figure 8 shows the photodegradation rates of DMP for WO<sub>3</sub>/TNAs photoelectrodes fabricated at various deposition times. The results indicated that the photodegradation rates of DMP increased with the deposition time when the time was shorter than 10 min. When the deposition time was over 15 min, the photodegradation rate of DMP decreased. This could be attributed to the excessive WO<sub>3</sub> sediment on the surface of TNAs

(Fig. 4), which inhibited the light absorption and the transfer of photogenerated carriers. The results were similar to those presented in Figs. 6 and 7.

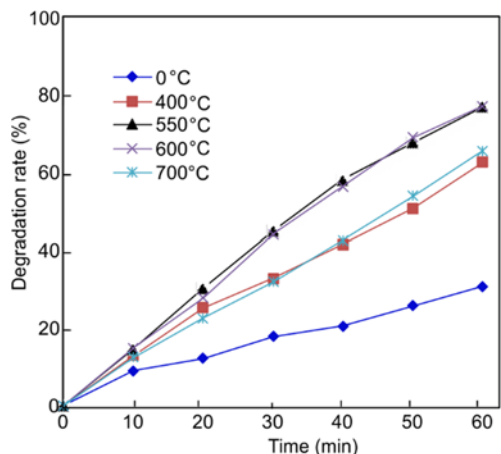


Fig. 9. Time dependences of the DMP photodegradation rate for  $\text{WO}_3/\text{TNAs}$  photoelectrodes fabricated at various annealing temperatures at  $\text{Na}_2\text{WO}_4$  concentration of  $0.01 \text{ mol/dm}^3$ , deposition time 10 min, deposition potential 3 V. The initial DMP concentration was  $20 \text{ mg/dm}^3$

The photodegradation rates of DMP for  $\text{WO}_3/\text{TNAs}$  photoelectrodes fabricated at various annealing temperatures are shown in Fig. 9.  $\text{WO}_3/\text{TNAs}$  photoelectrode without calcination displayed the lowest photodegradation rate of DMP after 60 min of illumination. The photodegradation rates of DMP for  $\text{WO}_3/\text{TNAs}$  photoelectrodes annealed at 400, 550, 600, and 700 °C reached 62.7, 77.1, 77.2 and 65.7%, respectively. The results verified that the  $\text{WO}_3/\text{TNAs}$  photoelectrode annealed at 550 and 600 °C performed excellent photocatalytic activity. The optimum photocatalytic performance was ascribed to the mixed crystal effect, which promoted the separation of photogenerated carriers [12, 26]. When the annealing temperature was 700 °C, the photodegradation rate of DMP decreased due to the collapse of nanotube array (Fig. 5e). The decrease caused the reduction of the specific surface area and was detrimental to the transfer of photogenerated electrons.

### 3.3. PHOTOCATALYTIC STABILITY OF $\text{WO}_3/\text{TNAs}$ PHOTOELECTRODES

The stability of  $\text{WO}_3/\text{TNAs}$  photoelectrode is a significant indicator for evaluation of its practical application. In order to evaluate the stability of  $\text{WO}_3/\text{TNAs}$  photoelectrode, the degradation efficiency of DMP was investigated by recycling the photoelectrodes for 10 cycles under irradiation for 60 min in each cycle. The stability and reusability of the  $\text{WO}_3/\text{TNAs}$  photoelectrodes is shown in Fig. 10. The removal efficiency of DMP was above 76% for all cycles. The experimental results indicated excellent chemical stability of  $\text{WO}_3/\text{TNAs}$  photoelectrodes, which could be ascribed to the formation of a robust coupling structure between  $\text{WO}_3$  and the TNAs.

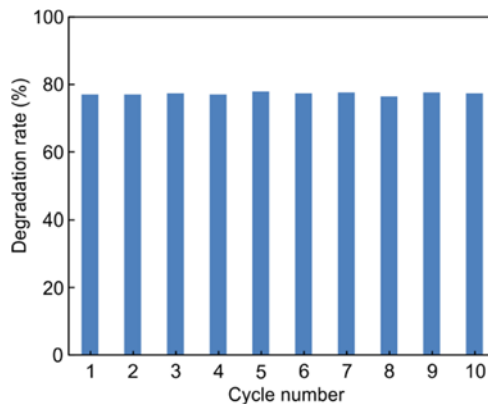


Fig. 10. The evolution of DMP photodegradation rate with the photodegradation cycles for WO<sub>3</sub>/TNAs photoelectrodes fabricated at Na<sub>2</sub>WO<sub>4</sub> concentration of 0.01 mol/dm<sup>3</sup>, deposition time 10 min, deposition potential 3 V, annealing temperature 550 °C, initial DMP concentration 20 mg/dm<sup>3</sup>, and 60 min illumination time for each cycle

#### 4. CONCLUSIONS

Various WO<sub>3</sub>/TNAs photoelectrodes were fabricated by the electrodeposition method on TNAs substrate. The results showed that suitable amount of WO<sub>3</sub> could improve the photocatalytic activity of TNAs photoelectrode. Under the 3.0 V deposition potential, 10 min deposition time, 0.01 mol/dm<sup>3</sup> Na<sub>2</sub>WO<sub>4</sub>, and 550 °C annealing temperature, the optimum photocatalytic performance of WO<sub>3</sub>/TNAs photoelectrode was achieved and the photodegradation rate of DMP reached 77% after 60 min of illumination. After reusing the WO<sub>3</sub>/TNA photoelectrodes 10 times, the photodegradation rate was still over 76%. The enhancement of photocatalytic performance by incorporating WO<sub>3</sub> onto TNAs would provide a theoretical basis for the practical application of WO<sub>3</sub>/TNA photoelectrodes in water treatment.

#### ACKNOWLEDGEMENTS

This work is supported by National Natural Science Foundation of China (No. 51208274, 51478490), China Postdoctoral Science Foundation (No. 2013M531651), and Natural Science Foundation of Shandong Province (No. ZR2012EEQ010, ZR. 2011EL044).

#### REFERENCES

- [1] HUNG C.H., YUAN C., LI H.W., *Photodegradation of diethyl phthalate with PANi/CNT/TiO<sub>2</sub> immobilized on glass plate irradiated with visible light and simulated sunlight-effect of synthesized method and pH*, J. Hazard. Mater., 2017, 322, 243.
- [2] CHANG C.F., MAN C.Y., *Magnetic photocatalysts of copper phthalocyanine-sensitized titania for the photodegradation of dimethyl phthalate under visible light*, Colloid. Surf. A, 2014, 441, 255.
- [3] CUI H., LIANG Z., ZHANG J.Z., LIU H., SHI J., *Enhancement of photocatalytic activity of TiO<sub>2</sub>/carbon aerogel based on hydrophilic secondary pore structure*, RSC Adv., 2016, 6 (72), 68416.

- [4] WANG Y., LIU Y., LIU T., SONG S., GUI X., LIU H., TSIKARAS P., *Dimethyl phthalate degradation at novel and efficient electro-Fenton cathode*, Appl. Catal. B: Environ., 2014, 156–157, 1.
- [5] SOUZA F.D., SAEZ C., CANIZARES P., MOTHEO A.D., RODRIGO M., *Electrochemical removal of dimethyl phthalate with diamond anodes*, J. Chem. Technol. Biotechnol., 2014, 89 (2), 282.
- [6] WANG J., WANG F., YAO J., WANG R., YUAN H., MASAKORALA K., CHOI M.M.F., *Adsorption and desorption of dimethyl phthalate on carbon nanotubes in aqueous copper(II) solution*, Colloid. Surf. A, 2013, 417, 47.
- [7] XU Z., CHENG L., SHI J., LU J., ZHANG W., ZHAO Y., LI F., CHEN M., *Kinetic study of the removal of dimethyl phthalate from an aqueous solution using an anion exchange resin*, Environ. Sci. Poll. Res., 2014, 21 (10), 6571.
- [8] XU L.J., CHU W., GRAHAM N., *A systematic study of the degradation of dimethyl phthalate using a high-frequency ultrasonic process*, Ultrason. Sonochem., 2013, 20 (3), 892.
- [9] SOUZA F.L., SAEZ C., CANIZARES P., MOTHEO A. J., RODRIGO M.A., *Sonoelectrolysis of wastewaters polluted with dimethyl phthalate*, Ind. Eng. Chem. Res., 2013, 52 (28), 9674.
- [10] ZHENG L., HAN S., LIU H., YU P., FANG X., *Hierarchical MoS<sub>2</sub> nanosheet@TiO<sub>2</sub> nanotube array composites with enhanced photocatalytic and photocurrent performances*, Small, 2016, 12 (11), 1527.
- [11] ESKANDARLOO H., HASHEMPOUR M., VICENZO A., FRANZ S., BADIEI A., BEHNAJADY M.A., BESTETTI M., *High-temperature stable anatase-type TiO<sub>2</sub> nanotube arrays. A study of the structure–activity relationship*, Appl. Catal. B: Environ., 2016, 185, 119.
- [12] XIN Y.J., LIU H.L., HAN L., ZHOU Y.B., *Comparative study of photocatalytic and photoelectrocatalytic properties of alachlor using different morphology TiO<sub>2</sub>/Ti photoelectrodes*, J. Hazard. Mater. 2011, 192 (3), 1812.
- [13] CAI J., HUANG J., GE M., IOCOZZIA J., LIN Z.Q., ZHANG K.Q., LAI Y.K., *Immobilization of Pt nanoparticles via rapid and reusable electropolymerization of dopamine on TiO<sub>2</sub> nanotube arrays for reversible SERS substrates and nonenzymatic glucose sensors*, Small, 2017, 13 (19), 1604240.
- [14] JANUS M., MARKOWSKA-SZCZUPAK A., KUSIAK-NEJMAN E., MORAWSKI A.W., *Disinfection of E. coli by carbon modified TiO<sub>2</sub> photocatalysts*, Environ. Prot. Eng., 2012, 38 (2), 89.
- [15] SUN M., MA X., CHEN X., SUN Y., CUI X., LIN Y., *A nanocomposite of carbon quantum dots and TiO<sub>2</sub> nanotube arrays: enhancing photoelectrochemical and photocatalytic properties*, RSC Adv., 2014, 4 (3), 1120.
- [16] CHENG X.W., LIU H.L., CHEN Q.H., LI J.J., WANG P., *Preparation and characterization of palladium nano-crystallite decorated TiO<sub>2</sub> nano-tubes photoelectrode and its enhanced photocatalytic efficiency for degradation of diclofenac*, J. Hazard. Mater. 254, 2013, 141.
- [17] WANG Q., QIAO J., ZHOU J., GAO S., *Fabrication of CuInSe<sub>2</sub> quantum dots sensitized TiO<sub>2</sub> nanotube arrays for enhancing visible light photoelectrochemical performance*, Electrochim. Acta, 2015, 167, 470.
- [18] ZHONG J.S., WANG Q.Y., ZHU X., CHEN D.Q., JI Z.G., *Solvothermal synthesis of flower-like Cu<sub>3</sub>BiS<sub>3</sub> sensitized TiO<sub>2</sub> nanotube arrays for enhancing photoelectrochemical performance*, J. Alloys Comp., 2015, 641, 144.
- [19] FENG H., TRAN.T.T., CHEN L., YUAN L., CAI Q., *Visible light-induced efficiently oxidative decomposition of p-Nitrophenol by CdTe/TiO<sub>2</sub> nanotube arrays*, Chem. Eng. J., 2013, 215, 591.
- [20] GAKHAR R., SMITH Y.R., MISRA M., CHIDAMBARAM D., *Photoelectric performance of TiO<sub>2</sub> nanotube array photoelectrodes sensitized with CdS 0.54 Se 0.46 quantum dots*, Appl. Surf. Sci., 2015, 355, 1279.
- [21] LU N., SU Y., LI J., YU H., QUAN X., *Fabrication of quantum-sized CdS-coated TiO<sub>2</sub> nanotube array with efficient photoelectrochemical performance using modified successive ionic layer absorption and reaction (SILAR) method*, Sci. Bull., 2015, 60 (14), 1281.

- 
- [22] MOMENI M.M., GHAYEB Y., DAVARZADEH M., *WO<sub>3</sub> nanoparticles anchored on titania nanotube films as efficient photoanodes*, Surf. Eng., 2015, 31, (4), 259.
- [23] XIE H., QUE W., HE Z., ZHONG P., LIAO Y., WANG G., *Preparation and photocatalytic activities of Sb<sub>2</sub>S<sub>3</sub>/TiO<sub>2</sub> nanotube coaxial heterogeneous structure arrays via an ion exchange adsorption method*, J. Alloys Comp., 2013, 550, 314.
- [24] XIN Y., LIU H., LIU Y., MA D.D., CHEN Q., *Composition and photoelectrochemical properties of WO<sub>3</sub>/TNAs photoelectrodes fabricated by in situ electrochemical method*, Electrochim. Acta, 2013, 104 (8), 308.
- [25] WANG G., CHEN Q., XIN Y., LIU Y., ZANG Z., HU C., ZHANG B., *Construction of graphene-WO<sub>3</sub>/TiO<sub>2</sub> nanotube array photoelectrodes and its enhanced performance for photocatalytic degradation of dimethyl phthalate*, Electrochim. Acta, 2016, 222, 1903
- [26] BEHNAJADY M.A., ALAMDARI M. E., MODIRSHAHLA N., *Investigation of the effect of heat treatment process on characteristics and photocatalytic activity of TiO<sub>2</sub>-UV100 nanoparticles*, Environ. Prot. Eng., 2013, 39 (1), 33.